Journal of Metals, Materials and Minerals, Vol. 29, No. 4, pp. 120-126, 2019

Electrodeposition of Zn/TiO_2 composite coatings for anode materials of Zinc ion battery

Kittima LOLUPIMAN[1,2], Panyawat WANGYAO[1,*], and Jiaqian QIN[2,*]

[1] *Metallurgical Engineering Department, Faculty of Engineering, Chulalongkorn University, Phayathai Road, Bangkok, 10330, Thailand*
[2] *Surface Coatings Technology for Metals and Materials Research Unit, Metallurgy and Materials Research Institute, Chulalongkorn University, Phayathai Road, Bangkok, 10330, Thailand*

[*]**Corresponding author e-mail:** jiaqian.q@chula.ac.th, panyawat.w@chula.ac.th

Received date:
24 October 2019
Revised date:
8 November 2019
Accepted date:
2 December 2019

Keywords:
Zn-ion battery
Zn anode
Electrodeposition
Plating-stripping
Specific capacity

Abstract

Researchers are paying more attention to Zinc ion battery (ZIB) because of the environment-friendly and low cost. However, the dendrite growth during cycling of Zn anode is still limited its long-term stability. Therefore, we report the electrodeposition of nano TiO_2 into Zn coatings and apply this composite coating for the anode materials of ZIBs. The Zn coatings and Zn/TiO_2 composite coatings in the electrolyte have been deposited on the stainless-steel foil and applied as the battery electrode. The plating/stripping testing in the symmetric cell demonstrate that the incorporation of TiO_2 into Zn coatings can decrease the overpotential between plating and stripping curves. In addition, nano flower MnO_2 as the cathode was synthesized by using hydrothermal method. The galvanostatic charge-discharge tests reveal that the Zn/TiO_2//MnO_2 aqueous batteries exhibit the higher rate ability and cycle performance than those of Zn//MnO_2 batteries.

1. Introduction

In recent years, many researchers are paying attention to the zinc ion battery (ZIB) for practical large-scale energy storage applications [1-4], because of abundant Zn source, low-cost, eco-friendly, etc. Zinc metal has low potential (-0.76 V vs. SHE), which is very suitable for the application of the anode in aqueous batteries. In addition, the high theoretical capacity (820 mA h g^{-1}) of Zn would be also good candidate for the lithium ion battery [1]. However, the poor cycle life and the inferior discharge performance usually hinder the ZIBs practical application [5], which is mainly caused by the growth of zinc dendrites during the charging-discharging process. Therefore, it is the important issue to solve the dendrite formation for ZIBs. Many researchers have proposed several methods to solve formation of Zn dendrite, such as modifying electrolyte formulation, additives, protective layer [6-13]. The additive used to inhibit the Zn dendrite is expensive and not cheap. Most of these protective layer approaches are still needed many steps to synthesis. Furthermore, the design of novel nanostructured anodes (e.g., 3D Zn oxide) were also developed to suppress the Zn dendrite growth [14-16]. However, the dendrite formation is still occurred during the cycling process and limits the ZIBs practical application. Therefore, the Zn dendrite suppression is still challenge for the practical applications of ZIBs.

Herein, the nano TiO_2 particles incorporated into Zn coatings (Zn/TiO_2) were applied on the Zn anode by co-electrodeposition method. The effect of TiO_2 on the microstructure was observed by scanning electron microscope (SEM). The symmetric Zn//Zn and Zn/TiO_2//Zn/TiO_2 cells were performed to evaluate the plating-stripping behavior. Furthermore, the full cells of Zn//MnO_2 and Zn/TiO_2//MnO_2 were fabricated to exam the battery performance for ZIBs.

2. Experimental

The Zn and Zn/TiO_2 coatings were fabricated by using facile electrodeposition method as shown in Figure1. The 500 ml beaker was used for the electroplating bath. Two-electrode cell with stainless steel foil (50*50mm, thickness 20 μm) as cathode and carbon steel plate as anode was applied for this work. The distance between two electrodes was 40 mm. The mixture solution of 125 $g \cdot L^{-1}$ of $ZnSO_4 \cdot 7H_2O$ (CARLOERBA), 125 $g \cdot L^{-1}$ of Na_2SO_4 (CARLOERBA), and 20 $g \cdot L^{-1}$ of boric acid (CARLOERBA) was applied for the pure Zn coatings. The Zn/TiO_2 coatings were prepared in the Zn coatings electrolyte with 10 $g \cdot L^{-1}$ of TiO_2 nanoparticles (25 nm, P25, Degussa) suspension. Before deposition, the stainless steel was etched in 14% HCl (CARLOERBA) and cleaned in the acetone and DI water with sonication. Both Zn and Zn/TiO_2 coatings were synthesized at the current density of 0.02 A cm^{-2} for 1h.

The MnO_2 was synthesized by using a hydrothermal method [17]. In brief, the 1.98 g of $KMnO_4$ (CARLOERBA) was dissolved in 60 mL DI water (solution A), 0.336 g of $MnSO_4 \cdot H_2O$ (CARLOERBA)

DOI: 10.14456/jmmm.2019.55

was dissolved in another 20 mL DI water (solution B). Then, the solution B was slowly added to the solution A, and stirred for 30 min. The obtained mixture was added into a 100 mL Teflon hydrothermal reactor and heated to 160 °C for 24 h in an oil bath. The final products were collected and washed, then dried at 80°C for overnight.

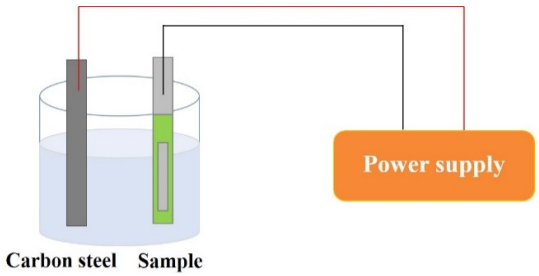

Figure 1. The electrodeposition setup.

The as-deposited coatings were studied by scanning electron microscope (SEM) on Hitachi S4800 to observe the surface morphology, and the phase was analyzed by X-ray diffraction (XRD) Rigaku D/MAX-Rb with Cu Kα radiation. The symmetric and full cells were assembled in a coin cells (CR2032) to test the plating/stripping and charging/discharging performance. The Zn and Zn/TiO_2 electrodes were punched with diameter of 14 mm. To exam the plating and stripping behavior, the Zn//Zn and Zn/TiO_2//Zn/TiO_2 cells were fabricated with glass fiber as separator, and the mixture solution of 2 M $ZnSO_4 \cdot 7H_2O$ and 0.1 M $MnSO_4$ was applied as electrolyte. The galvanostatic charge-discharge (GCD) cycling was carried out in the Neware (Shenzhen, China) battery system. The testing parameters are the constant current density of 0.5 mA cm^{-2} for 30 min during each charge and discharge step.

To exam the ZIBs properties of the Zn//MnO_2 and Zn/TiO_2//MnO_2 cells, galvanostatic charge-discharge (GCD) method was used at various current density of 50, 100, 200, 500, 1000 mA g^{-1} in the voltage window of 0.6-1.7 V. The cathode was prepared by 70 wt.% of MnO_2, 20 wt.% of acetylene back, and 10 wt.% polyvinylidene (PVDF) in the N-methyl-2-pyrrolidone solvent. The slurry was cast onto a graphite paper, then dried at 80°C for 12 h under vacuum. The full cells were assembled with Zn and Zn/TiO_2 coatings as anode, MnO_2 cathode and glass fiber separator.

3. Results and discussion

The Zn and Zn/TiO_2 coatings can be successfully deposited. Figure 2 shows the SEM images of Zn coatings and Zn/TiO_2 coatings. The morphology differences of pure Zn coatings and the Zn coatings with incorporation of TiO_2 nanoparticles can be clearly observed in the Figure 2(a-d). The Zn coating (Figure 2(a)) exhibits large granular, big gap, and coarse surface, the large magnification image (Figure 2(b)) further reveals that the sharp needles grow on the surface of granular. The gray spots in the SEM images (Figure 2(c, d)) indicate that the TiO_2 particles could be inserted into the Zn coatings with the suspension of TiO_2 nanoparticles in the electrolyte of Zn coatings. Furthermore, the introduced TiO_2 nanoparticles can also make the Zn coatings smooth and compact, inhibit the formation of sharp needles. The suspension of nanoparticles in the electrolyte can lead to the increasing in the number of crystal nucleation, slow the growth of crystalline grain and reduce the grain size. Therefore, the incorporation of TiO_2 nanoparticles can significantly fine the granular size, obtain the smooth surface, and generate the compact morphology (Figure 2).

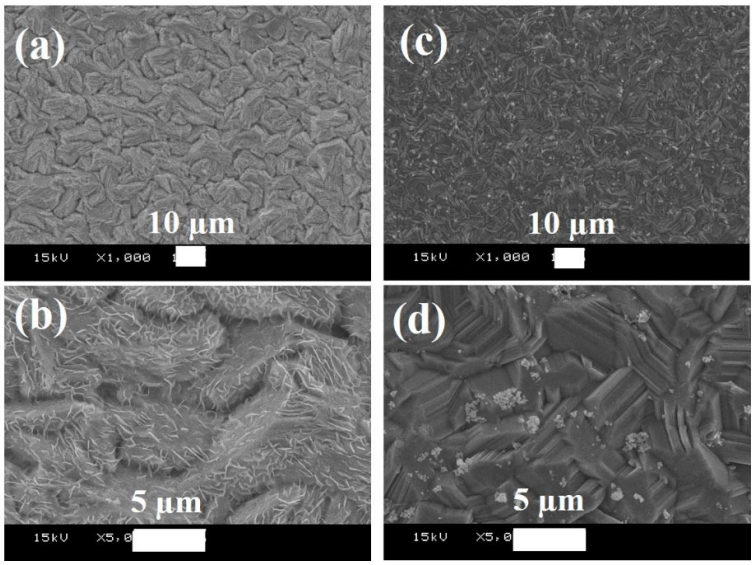

Figure 2. SEM images of Zn coatings (a, b) and Zn-TiO2 composite coatings (c, d).

The magnified observation of Zn/TiO_2 coatings (Figure 2(d)) shows the compact, smooth, and small granular size of Zn coatings. During the co-electrodeposition, the TiO_2 nanoparticles would be adsorbed onto the surface of Zn coatings, which will reduce the coating surface area and provide higher current density in comparison with pure Zn electrodeposition. The higher current density can contribute to the large cathode over-potential, which can increase the crystalline nucleus formation probability [18]. Therefore, the introduced TiO_2 nanoparticles could decrease the grain size of deposition, resulting the small granular size, smooth surface and compact coatings.

The XRD was also applied to confirm the deposits of Zn and Zn/TiO_2 coatings as shown in Figure 3. Both diffraction patterns can be indexed to the Zn (JCPDS No. 99-0090), and TiO_2 (JCPDS No. 99-0110) can be also detected in the Zn-TiO_2 coatings. Thus, both SEM and XRD can demonstrate that the Zn and Zn/TiO_2 coatings can be successfully deposited by using electrodeposition method.

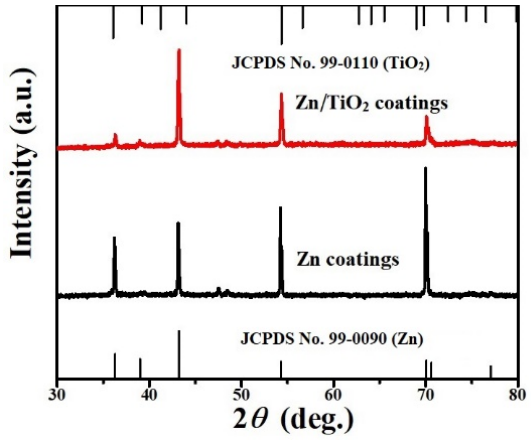

Figure 3. XRD patterns of Zn and Zn-TiO_2 coatings.

Zn plating/stripping performances of Zn//Zn and Zn/TiO_2//Zn/TiO_2 electrodes were performed by GCD method in a symmetric 2032 cell. At current density of 0.5 mA cm^{-2}, the plating/stripping processes of Zn//Zn and Zn/TiO_2//Zn/TiO_2 are shown in Figure 4. The results demonstrate that both Zn//Zn and Zn/TiO_2// Zn/TiO_2 can operate steadily over 500 cycles without the short circuit. However, the incorporation of TiO_2 nanoparticles can reduce the overpotential between plating and stripping curves (Figure 4(a, b)). During the cycling, the Zn/TiO_2//Zn/TiO_2 cells can show much more flat voltage plateau than those of Zn//Zn cells, while the overpotential between plating and stripping of Zn//Zn cells slightly increases.

According to the characterized results, the schematic of the plating/stripping can be proposed as shown in Figure 5. Without the TiO_2 nanoparticles, the gaps around the granular boundaries and sharp needle can be observed on the surface of Zn coatings (Figure 5(a)), while the compact and smooth surface can be obtained for the Zn/TiO_2 coatings (Figure 5(b)). During the plating/stripping process, Zn will be stripped and dissolved into the electrolyte, then plated back onto the Zn electrode. The Zn dendrite is generated during the dissolved Zn cations coating back onto Zn electrode with the applied current. Because the Zn coatings have many defects such as sharp edges, coarse surface, and big gaps around the granular boundaries, the distribution of current will be not uniform on the coarse surface of Zn coatings. The sharp points with high current area tend to deposit faster and much coarse than other flat area, resulting in the dendrite formation on the Zn coatings electrode (Figure 5(c)). While the Zn/TiO_2 coatings exhibit a compact and smooth surface, the current distribution would be uniform and then can keep flat surface during the cycle process (Figure 5(d)). To confirm this proposed mechanism, the morphology of electrode after plating/stripping was observed by using SEM (Figure 5(e,f)). For the Zn electrode, the dendrite can be clearly seen (Figure 5(e)), while the Zn/TiO_2 electrode still exhibit the smooth and compact surface. The results further demonstrate that the addition of TiO_2 can effectively suppress the formation of dendrite during plating/stripping. This can make the Zn/TiO_2 as the potential anode materials for ZIBs.

To exam the practical application of our strategy, the full ZIBs prototype was assembled. In this work, the Zn//MnO_2 and Zn/TiO_2//MnO_2 2032-coin cells were fabricated using a MnO_2 as cathode materials. The MnO_2 can be synthesized by using hydrothermal method, which can be determined by XRD and SEM (Figure 6). XRD patterns (Figure 6(a)) of the synthesized MnO_2 can match well with the MnO_2 (JCPDS No. 00-050-0866). SEM was also carried out to study the morphology of the synthesized MnO_2 as shown in Figure 6(b), which demonstrates that the nanoflower cluster microstructures MnO_2 can be obtained. The nanoflower cluster with diameter of ~400 nm can be constructed by the nanosheet with the thickness~5 nm. The obtained nanoflower cluster with many pores among the nanosheets can improve the contact area between the electrode materials and electrolyte and result the fast ion transfer in the charge/discharge process [19].

GCD measurements were charged/discharged in the electrolyte (mixture solution of 2 M $ZnSO_4$ and 0.1 M $MnSO_4$) to evaluate the full cell performance at different current densities (Figure 7). To suppress the dissolution of Mn^{2+} from the cathode, $MnSO_4$ additive was also added in the electrolyte [20]. The GCD results show that the charge/discharge efficiency of Zn/TiO_2//MnO_2 cells rapidly rise to ~100%, and it can keep almost constant at all current densities. While the

charge/discharge efficiency of Zn//MnO_2 cells can only reach up to ~98% for various current densities.

The Zn/TiO_2//MnO_2 ZIBs can obtain capacities of 168, 131, 115, 78, 49 mAh·g^{-1} under current density of 50, 100, 200, 500, and 1000 mA·g^{-1}, respectively (Figure 7(a)). In comparison, the Zn//MnO_2 batteries only provide capacities of 110, 89, 67, 38, 15 mAh·g^{-1} under current density of 50, 100, 200, 500, and 1000 mA·g^{-1}, respectively (Figure 7(b)). In comparison with the pure Zn anode, the GCD results demonstrate that the induced TiO_2 nanoparticles can significantly improve the capacities about 52%, 47%, 72%, 105%, and 227% at current density of 50, 100, 200, 500, and 1000 mA·g^{-1}, respectively. The rate capability of Zn/TiO_2//MnO_2 is significantly higher than those of Zn//MnO_2 batteries, as shown in Figure 7(a,b). Moreover, when the rate switched back to 200 mA·g^{-1}, the capacity 100 mAh·g^{-1} can be recovered.

The cycle stability was also examined as shown in Figure 7(c,d), after 50 charging and discharging cycles, the capacity retention is about 83% for the Zn/TiO_2//MnO_2 batteries (Figure 7(c)), while the capacity retention is only 62% for the Zn//MnO2 batteries (Figure 7(d)).

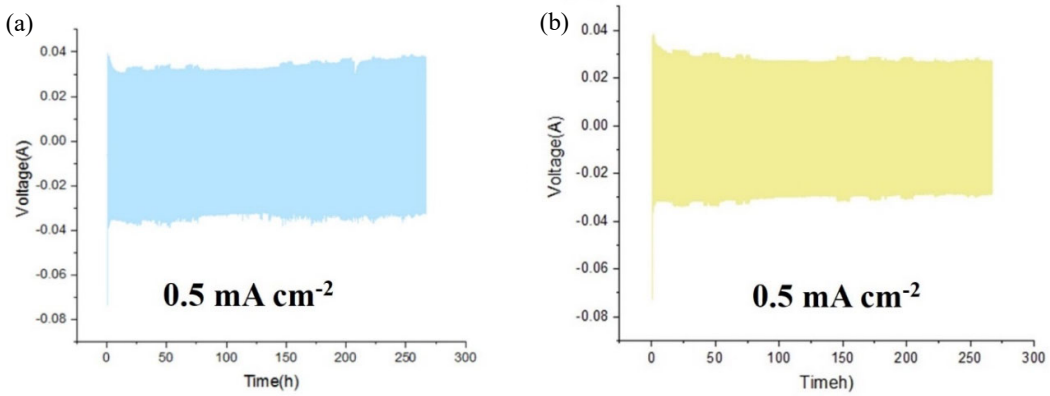

Figure 4. Plating/stripping performance of Zn//Zn and Zn-TiO_2//Zn-TiO_2 symmetric cells at a current density of 0.5 mA cm^{-2}.

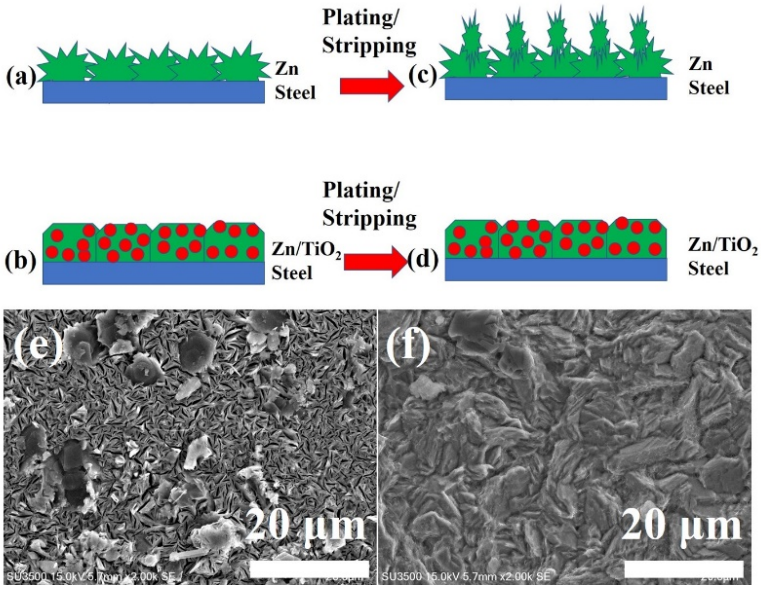

Figure 5. The schematic of as-deposited Zn (a) and Zn-TiO_2 (b) and after plating/stripping of Zn (c) and Zn-TiO_2 (d).

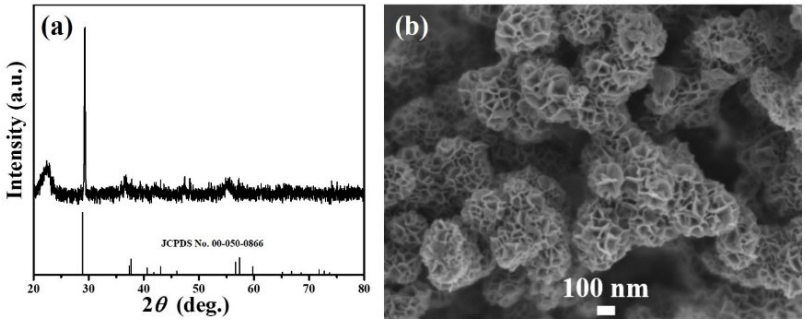

Figure 6. XRD pattern of synthesized MnO_2 (a) and SEM image (b).

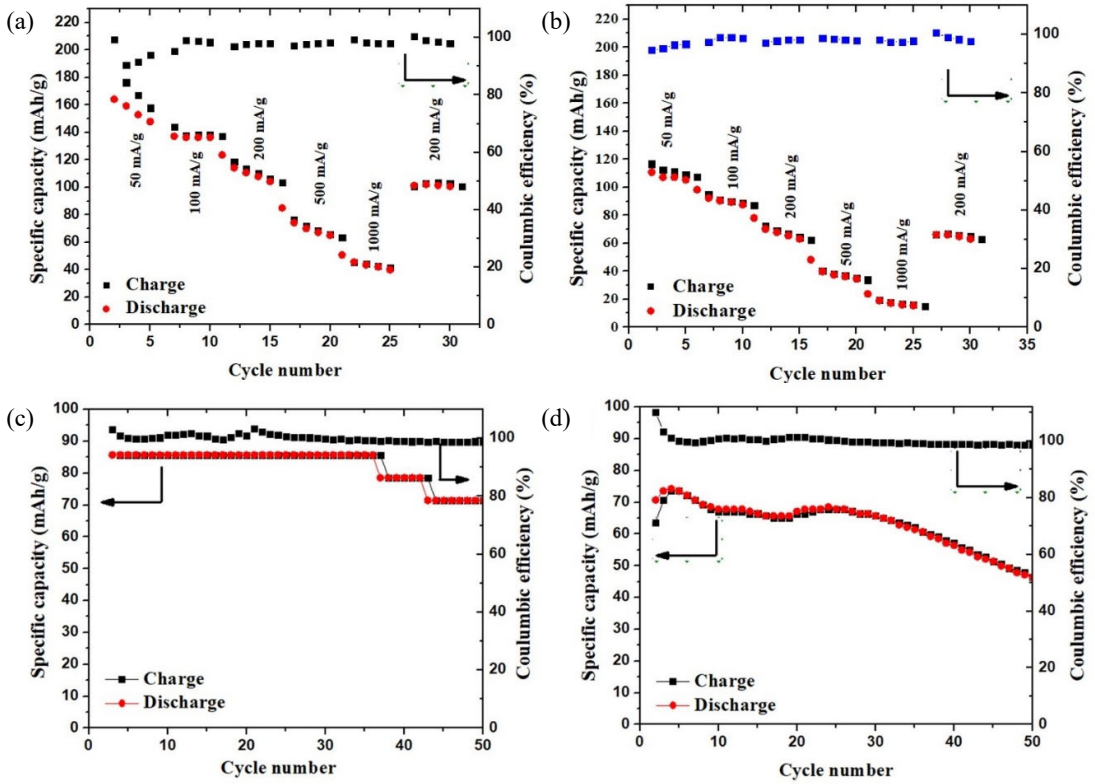

Figure 7. Rate capability at different current densities and Coulombic efficiency for Zn-TiO_2//MnO_2 (a) and Zn//MnO_2 (b). Cycle capability and Coulombic efficiency for Zn-TiO_2//MnO_2 (a) and Zn//MnO_2 for 50 cycles.

4. Conclusions

In this work, one facile electrodeposition method of synthesizing inexpensive Zn/TiO_2 composite coatings has been introduced. The incorporation of TiO_2 into Zn coatings can improve the plating/stripping performance of symmetric Zn//Zn cells, which can decrease the overpotential between plating and stripping curves. In addition, the nano flower MnO_2 was synthesized by using hydrothermal method and applied as the cathode, the Zn/TiO_2//MnO_2 aqueous batteries were constructed for the first time. In comparison with Zn//MnO_2 batteries, Zn/TiO_2//MnO_2 aqueous exhibit high specific capacity, high rate ability, and better cycle performance. This novel and facile design could be possible applied for the future practical applications, and thus further studies are needed.

5. Acknowledgements

This work is supported by the Energy Conservation Promotion Fund from and the Energy Policy and Planning Office, Ministry of Energy, K. L.

and J. Q. gratefully acknowledge the financial support from the TRF-IRN Program granted to the International Research Network on Electroplating Technology (IRN61W0002) and Thailand Research Fund (RSA6080017).

References

[1] Q. Fang, B. Song, T.-T. Tee, L. T. Sin, D. Hui, and S.-T. Bee, "investigation of dynamic characteristics of nano-size calcium carbonate added in natural rubber vulcanizate," *Composites Part B: Engineering,* vol. 60, pp. 561-567, 2014.

[2] M. M. Kamal, J. Clarke, and M. A. Ahmad, "Comparison of properties of natural rubber compounds with various fillers," *Journal of Rubber Research,* vol. 12(1), pp. 27-44, 2009.

[3] I. Khan and A. Bhat, "Micro and nano calcium carbonate filled natural rubber composites and nanocomposites," in: *RSC Polymer Chemistry Series No. 8 Natural Rubber Materials, Volume 2: Composites and Nanocomposites.* Ed. by S. Thomas, H. J. Maria, J. P. Joy, C. H. Chan, and L. A. Pothen, London: Royal Society of Chmistry, 2014, vol. 2, pp. 467-487.

[4] C. Wang, J. Zhao, X. Zhao, H. Bala, and Z. Wang, "Synthesis of nanosized calcium carbonate (aragonite) via a polyacrylamide inducing process.," *Powder Technology*, vol. 163, pp. 134-138, 2006.

[5] L. Liang, Y. C. Lam, K. C. Tam, T. H. Chua, G. W. Sim, and L. S. Ang, "Strengthening acrylonitrile-butadiene-styrene (ABS) with nano-sized and micron-sized calcium carbonate," *Polymer,* vol. 46, pp. 243-252, 2005.

[6] S. Manroshan and A. Baharin, "Effect of nanosized calcium carbonate on the mechanical properties of latex films," *Journal of Applied Polymer Science*, vol. 96, pp. 1550-1556, 2005.

[7] S. S. Fernandez and S. Kunchandy, "Comparative study of the cure and mechanical properties of natural rubber/expandable graphite vulcanizate filled with nano and precipitated calcium carbonate," *Asian Journal of Chemistry,* vol. 25(15), pp. 8638-8642, 2013.

[8] S. Attharangsan, H. Ismail, M. A. Bakar, and J. Ismail, "Carbon black (CB)/rice husk powder (RHP) hybrid filler-filled natural rubber composites: effect of CB/RHP ratio on property of the composites," *Polymer-Plasts Technology and Engineering,* vol. 51(7), pp. 655-662, 2012.

[9] S. Prasertsri, C. Vudjung, I. Wunchai., S. Srichan, K. Sapprasert, and J. Kongon, "Comparison of reinforcing efficiency between calcium carbonate/carbon black and calcium carbonate/silica hybrid filled natural rubber composites," *Defect and Diffusion Forum,* vol. 382, pp. 94-98, 2018,

[10] A. Oyetunji, R. Umunakwe, B. O. Adewuyi, U. S. Nwigwe, and I. J. Umunakwe, "Evaluating the properties of nanoparticles of calcium carbonate obtained from the shells of african giant land snails (*Achatina achatina*) via *in situ* deposition technique," *UPB Scientific Bulletin: Series B Chemistry and Materials Science,* vol 81(1), pp. 85-94, 2019.

[11] ASTM D 3184-89, "Standard Test Method for Rubber-Evaluation of Natural Rubber (Natural Rubber)," in: *Annual Book of ASTM Standards, ASTM International,* West Conshohocken, USA, 1989.

[12] ASTM D 412-06a, "Standard Test Methods for Vulcanized Rubber and Thermoplastic Elastomers—Tension," in: *Annual Book of ASTM Standards, ASTM International,* West Conshohocken, USA, 2006.

[13] ISO 7619-1:2010, "Rubber, Vulcanized or Thermoplastic—Determination of Indentation Hardness—Part 1: Durometer Method (Shore hardness)," *ISO Standard,* 2010.

[14] ISO 4649:2010 (E), "Rubber, Vulcanized or Thermoplastic - Determination of Abrasion Resistance using a Rotating Cylindrical Drum Device," *ISO Standard,* 2010.

[15] ASTM D D 395 – 03 (2003), "Standard Test Methods for Rubber Property—Compression Set," in: *Annual Book of ASTM Standards, ASTM International,* West Conshohocken, USA, 2003.

[16] I. O. Igwe and A. A. Ejim, "Studies on mechanical and end-use properties of natural rubber filled with snail shell powder," *Materials Sciences and Application,* vol. 2, pp. 802-810, 2011.

[17] H. Norazlina, A. R. M. Fahmi, and W. M. Hafizuddin, "$CaCO_3$ from sea shells as a reinforcing filler for natural rubber," *Journal of Mechanical Engineering and Sciences,* vol. 8, pp. 1481-1488, 2015.

[18] M. Galimberti, V. Cipolletti, and V. Kuma, "Nanofillers in natural rubber," in: *Natural Rubber Materials: Volume 2: Composites and Nanocomposites*. Ed. by S. Thomas, C. H. Chan, L. Pothen, J. Joy, and H. Maria. *Royal Society of Chemistry,* 2014, ISBN:978-1-84973-631-2, Cambridge, United Kingdom.

[19] G. Heinrich, and T. A. Vilgis, "Contribution of entanglements to the mechanical properties of carbon blackfilled polymer networks", *Macromolecules*, vol. 26, pp. 1109-1119, 1993.

[20] J.-B. Donnet, and E. Custodero, (2013). "Reinforcement of elastomers by particulate fillers," in: *The Science and Technology of Rubber 4th Edition*. Ed by J. E. Mark, B. Erman, and R. C. Michael. Elsevier Inc., Amsterdam, 2014, pp. 383-416.

[21] F. M. Nejad, M. Tolouei, H. Nazari, and A. Naderan, A., "Effects of calcium carbonate nanoparticles and fly ash on mechanical and permeability properties of concrete," *Advances in Civil Engineering Materials,* vol. 7(1), pp. 651-668, 2018.

[22] Z. H. Li, J. Zhang, and S. J. Chen, "Effects of carbon blacks with various structures on vulcanization and reinforcement of filled ethylene-propylene-diene rubber", *eXPRESS Polymer Letters*, vol. 2(10), pp. 95-704, 2008.

[23] Z. G. Abdulkadhim, "Influence calcium carbonate nano-particles $CaCO_3$ on mechanical properties for NR compound," *International Journal of Mechanical and Mechatronics Engineering,* vol. 14(2), pp. 114-117, 2014.

[24] J. Johns, and V. L. Rao, "Thermal stability, morphology and x-ray diffraction studies on dynamically vulcanized natural rubber chitosan blend," *Journal of Materials Science,* vol. 44, pp. 4087-4094, 2009.

[25] I. L. Haridan, "*A Comparative Study of Natural Rubber Modified with Ground Tire Rubber of Truck".* Barcelona: Universitat Politecnica de Catalunya, 2016.

[26] J. T. Varkey, S. Augustine, and S. Thomas, "Thermal deegrdation of natural rubber/styrene butadiene rubber latex blend blends by themogravimetric method," *Polymer-Plastics Technology and Engineering*, vol. 39(3), pp. 415-435, 2000.